JACS
JOURNAL OF THE AMERICAN CHEMICAL SOCIETY
Article
pubs.acs.org/JACS

A Series of Simple Oligomer-like Small Molecules Based on Oligothiophenes for Solution-Processed Solar Cells with High Efficiency

Bin Kan,[†,⊥] Miaomiao Li,[†,⊥] Qian Zhang,[†,⊥] Feng Liu,[‡] Xiangjian Wan,[†] Yunchuang Wang,[†] Wang Ni,[†] Guankui Long,[†] Xuan Yang,[†] Huanran Feng,[†] Yi Zuo,[†] Mingtao Zhang,[∥] Fei Huang,[§] Yong Cao,[§] Thomas P. Russell,[‡] and Yongsheng Chen*[,†]

[†]State Key Laboratory and Institute of Elemento-Organic Chemistry and Centre for Nanoscale Science and Technology, Institute of Polymer Chemistry and Collaborative Innovation Center of Chemical Science and Engineering (Tianjin), College of Chemistry, Nankai University, Tianjin 300071, China

[‡]Polymer Science and Engineering Department, University of Massachusetts, Amherst, Massachusetts 01003, United States

[§]State Key Laboratory of Luminescent Materials and Devices, South China University of Technology, Guangzhou 510640, China

[∥]Computational Center for Molecular Science, College of Chemistry, Nankai University, Tianjin 300071, China

Supporting Information

ABSTRACT: A series of acceptor−donor−acceptor simple oligomer-like small molecules based on oligothiophenes, namely, DRCN4T−DRCN9T, were designed and synthesized. Their optical, electrical, and thermal properties and photovoltaic performances were systematically investigated. Except for DRCN4T, excellent performances were obtained for DRCN5T−DRCN9T. The devices based on DRCN5T, DRCN7T, and DRCN9T with axisymmetric chemical structures exhibit much higher short-circuit current densities than those based on DRCN6T and DRCN8T with centrosymmetric chemical structures, which is attributed to their well-developed fibrillar network with a feature size less than 20 nm. The devices based on DRCN5T/$PC_{71}BM$ showed a notable certified power conversion efficiency (PCE) of 10.10% under AM 1.5G irradiation (100 mW cm^{-2}) using a simple solution spin-coating fabrication process. This is the highest PCE for single-junction small-molecule-based organic photovoltaics (OPVs) reported to date. DRCN5T is a rather simpler molecule compared with all of the other high-performance molecules in OPVs to date, and this might highlight its advantage in the future possible commercialization of OPVs. These results demonstrate that a fine and balanced modification/design of chemical structure can make significant performance differences and that the performance of solution-processed small-molecule-based solar cells can be comparable to or even surpass that of their polymer counterparts.

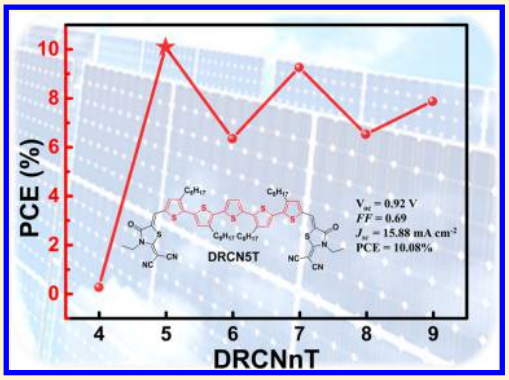

INTRODUCTION

Organic photovoltaics (OPVs) are considered a promising solar energy conversion technology having the advantages of being solution-processable, lightweight, low-cost, and flexible.[1] With the rapid progress in the past decade, power conversion efficiencies (PCEs) of over 10% have been achieved for polymer-based OPVs (P-OPVs) with bulk heterojunction (BHJ) architectures.[2−6] This progress has occurred as a result of the development of photoactive materials, including electron-donor[7−11] and electron-acceptor materials,[12,13] along with innovations and optimizations in device processing.[14−19] Compared with the widely investigated P-OPVs,[20−23] solution-processed small-molecule-based OPVs (SM-OPVs) have made great strides recently,[24,25] and PCEs near 10%[26] have been achieved for single-junction solar cells and over 10% for tandem devices,[27] which are comparable to the performance of P-OPVs. In view of the advantages of small molecules, including well-defined but versatile chemical structures, allowing easier energy level control, mobility tuning, and no batch-to-batch variations,[28] they are good candidates not only for understanding the relationships between molecular structure and device performance but also for achieving higher OPV performance.[29,30]

For the design of donor materials, it is necessary to strike a delicate balance between solubility, absorption over a broad wavelength range, suitable energy levels, and high mobility. Combining electron-deficient end groups (acceptor) and an electron-rich central unit (donor) to form an acceptor−donor−acceptor (A−D−A) type of small molecules is one of the more successful and effective strategies to tune the absorption and energy levels and achieve high performance.[31,32] Oligothio-

Received: January 11, 2015
Published: March 4, 2015

DOI: 10.1021/jacs.5b00305
J. Am. Chem. Soc. 2015, 137, 3886−3893

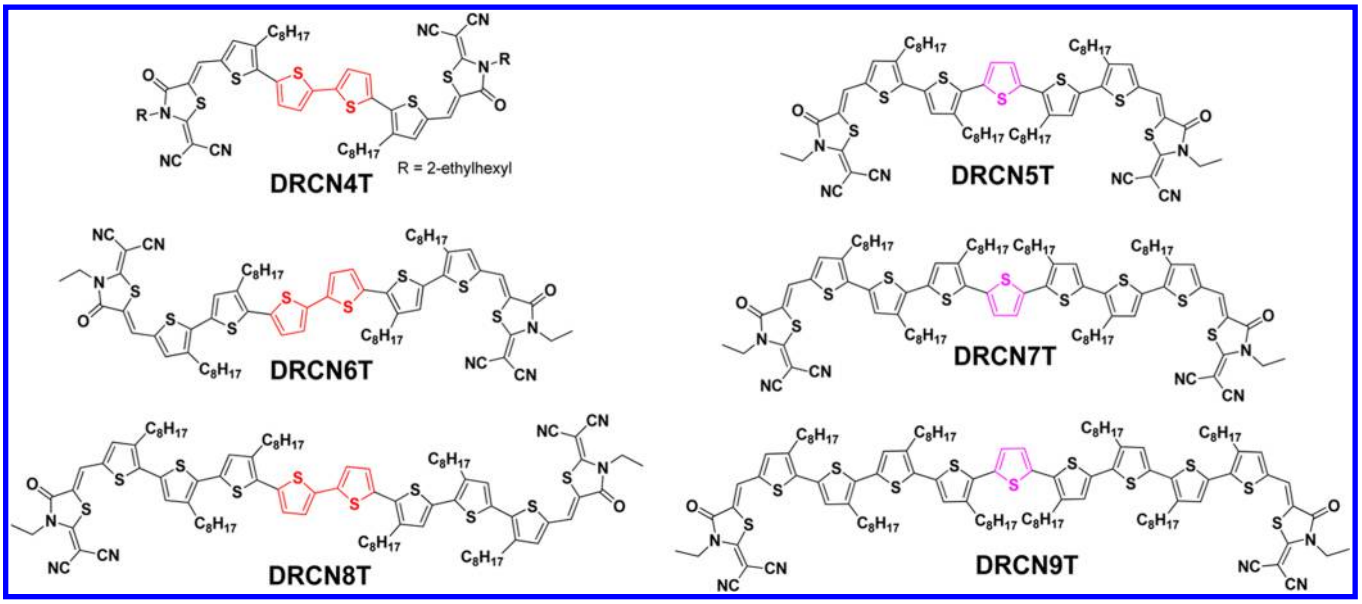

Figure 1. Chemical structures of DRCN4T−DRCN9T.

Scheme 1. Synthesis Routes for DRCN4T−DRCN9T

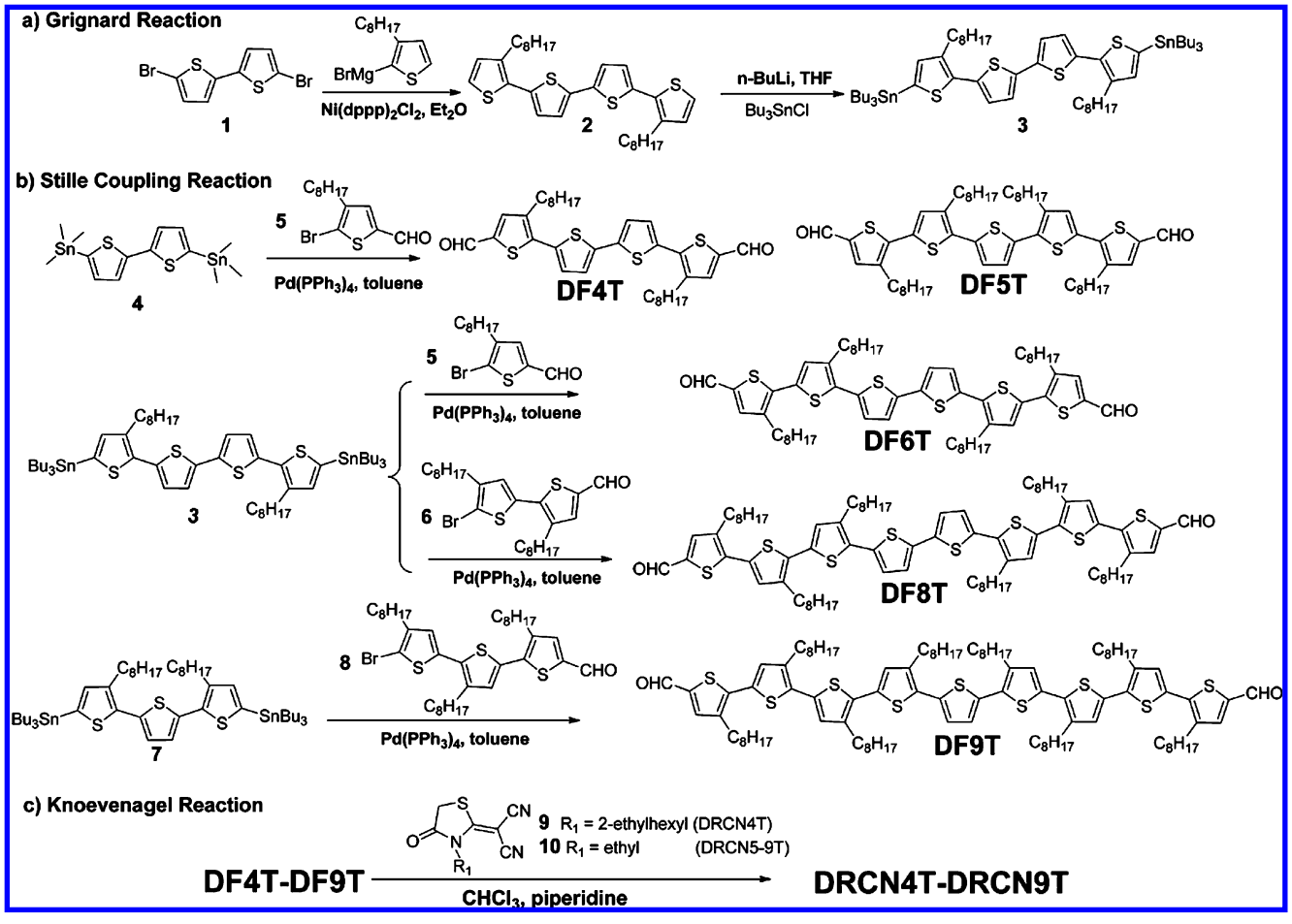

phenes are among the most highly investigated organic semiconductor materials and have been widely used in OPVs because of their excellent charge transport properties, high polarizability, and tunable optical/electrochemical properties together with their relatively simple synthesis, easy access, and high stability.[33−37] Just recently, we reported DRCN7T, a linear A−D−A small molecule containing septithiophenes as the backbone with 2-(1,1-dicyanomethylene)rhodanine as the end groups, which achieved outstanding OPV performance with a PCE of 9.30%.[38] It has been reported that conjugation length and spatial symmetry have a significant impact on the molecular orbital energy levels, molecular packing, phase separation, and

DOI: 10.1021/jacs.5b00305
J. Am. Chem. Soc. 2015, 137, 3886−3893

charge carrier mobility.[39−43] Whether the conjugation length of DRCN7T is optimal and how the conjugation length and the spatial symmetry of small molecules affect their properties need to be comprehensively investigated.

In this work, a series of A−D−A small molecules, namely, DRCN4T−DRCN9T (Figure 1), with the same end groups and similar backbones but different conjugation lengths and spatial symmetry, were designed and synthesized. Their OPV performances were systematically investigated together with that of DRCN7T for comparison. DRCN5T, DRCN7T, and DRCN9T, which have an axisymmetric structure and therefore larger dipole moment differences ($\Delta\mu_{ge}$) between the ground (μ_g) and excited states (μ_e), have a better-developed fibrillar network in the active layers, a much higher short-circuit current density (J_{sc}), and higher PCEs than the corresponding centrosymmetric DRCN4T, DRCN6T, and DRCN8T. Very low photovoltaic performance was found for the devices based on DRCN4T because of the poor quality of the films. However, the devices based on all of the compounds DRCN5T−DRCN9T yielded good photovoltaic performances with PCEs of over 6%. Importantly, a notable certified PCE of 10.10% was achieved for the device based on the simple molecule DRCN5T, which is the highest PCE for single-junction SM-OPVs reported to date.

RESULTS AND DISCUSSION

Synthesis and Thermal Properties. Figure 1 shows the chemical structures of the targeted molecules DRCN4T−DRCN9T, and the synthetic routes are shown in Scheme 1. The important intermediates DF5T and compounds **5**−**10** in Scheme 1 were prepared according to our previous work.[33,34] Via simple Grignard and Stille coupling reactions, DF4/6/8/9T were obtained as red solids. The targeted molecules were then synthesized by the Knoevenagel condensation of DF4T−DF9T with compound **9** or **10** in high yields. The detailed syntheses and characterization data are provided in the Supporting Information (SI). These A−D−A molecules possess different conjugation lengths with the same end groups and similar backbones, which are composed of thiophene units and easily synthesized. Purification using conventional chromatography with silica gel and then recrystallization from $CHCl_3$ offered the final products with high purity, as is necessary for OPV device fabrication. The optimized geometries of DRCN4T−DRCN9T, based on density functional density (DFT) calculations, are presented in Figure S1 in the SI.[44] DRCN4T, DRCN6T, and DRCN8T are centrosymmetric and DRCN5T, DRCN7T, and DRCN9T are axisymmetric, consistent with the X-ray crystal results for other similar molecules based on oligothiophenes.[45−47] All of these molecules exhibit good solubility in common organic solvents and excellent thermal stability up to 360 °C under a nitrogen atmosphere by thermogravimetric analysis (TGA) (Figure S2a in the SI). Differential scanning calorimetry (DSC) analysis (Figure S2b and Table S2 in the SI) was used to investigate thermal transitions of their solid states. Clear melting temperatures (T_m) upon heating and recrystallization points (T_{cr}) upon cooling are observed for these molecules, indicating that these molecules can readily crystallize, as also evidenced by grazing-incidence X-ray diffraction (GIXD).

Optical Absorption and Electrochemical Properties. The solution and normalized thin-film optical absorption spectra of DRCN4T−DRCN9T are presented in Figure 2a,b, and some important optical data are listed in Table 1. In dilute

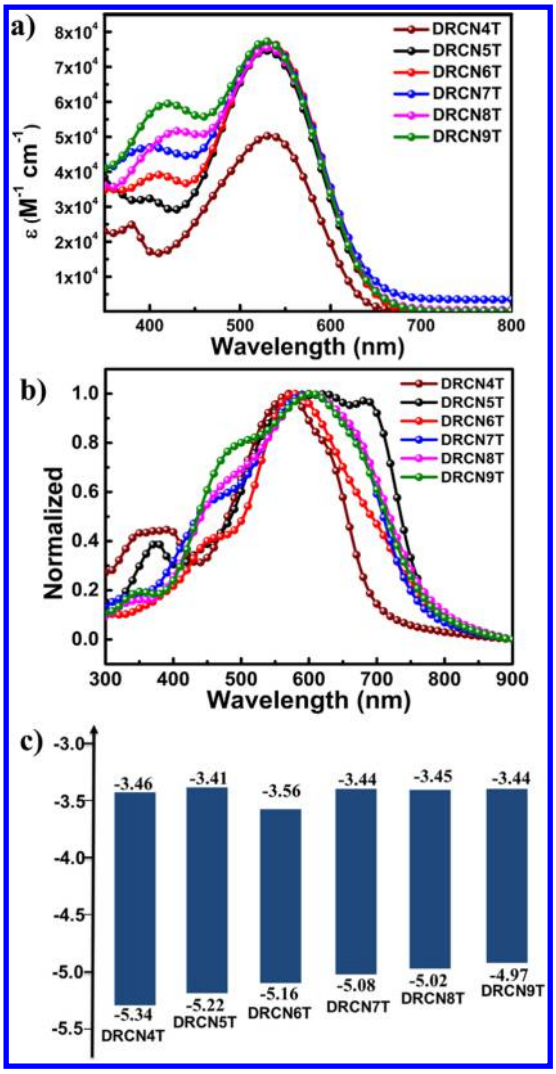

Figure 2. (a) UV−vis absorption spectra of DRCN4T−DRCN9T solutions. (b) UV−vis absorption spectra of DRCN4T−DRCN9T films. (c) HOMO and LUMO energy levels of DRCN4T−DRCN9T.

chloroform solution, these molecules show an absorption peak at ∼531 nm independent of their conjugation length and symmetry. Meanwhile, the maximal absorption coefficients of DRCN5T−DRCN9T are similar and are much higher than that of DRCN4T. The reason for the similar absorption of DRCN5T−DRCN9T may be that the effective conjugation lengths of these molecules have been achieved by five thiophene units together with the two conjugated end units.[37,42] In the solid state, all of the molecules display an obvious red-shifted and broad absorption compared with their solution absorption. However, DRCN4T exhibits a narrower absorption compared with the other molecules, probably because of its shorter conjugation length. Their thin-film spectra show different patterns, indicating possible differences in molecular aggregation in the solid state. It is noteworthy that the DRCN5T film shows a broader absorption and a distinct shoulder at 685 nm, indicating more effective molecular packing between molecular backbones. The optical band gaps of DRCN4T−DRCN9T estimated from the onset of the film absorption are 1.77, 1.60, 1.60, 1.62, 1.61, and 1.59 eV, respectively. Cyclic voltammetry (CV) was used to investigate the energy levels of DRCN4T−DRCN9T (Figure S3 in the SI).

DOI: 10.1021/jacs.5b00305
J. Am. Chem. Soc. 2015, 137, 3886−3893

Table 1. Optical and Electrochemical Data of Compounds DRCN4T−DRCN9T

	solution		film			CV				
molecule	$\varepsilon(\lambda_{max})$ (M^{-1} cm^{-1})	λ_{max} (nm)	λ_{max} (nm)	λ_{onset} (nm)	E_g^{opt} (eV)	E_{onset}^{ox} (V)	E_{onset}^{red} (V)	E_{HOMO} (eV)	E_{LUMO} (eV)	E_g^{elec} (eV)
DRCN4T	5.0×10^4	532	573	700	1.77	0.54	−1.34	−5.34	−3.46	1.88
DRCN5T	7.5×10^4	531	583, 685	777	1.60	0.42	−1.39	−5.22	−3.41	1.81
DRCN6T	7.6×10^4	532	577	775	1.60	0.36	−1.24	−5.16	−3.56	1.60
DRCN7T	7.8×10^4	530	602	764	1.62	0.28	−1.36	−5.08	−3.44	1.64
DRCN8T	7.5×10^4	531	602	771	1.61	0.22	−1.35	−5.02	−3.45	1.57
DRCN9T	7.7×10^4	530	603	788	1.59	0.17	−1.36	−4.97	−3.44	1.53

Table 2. Average OPV Performance Parameters for DRCN5T−DRCN9T BHJ Devices under the Optimized Conditions

molecule	V_{oc} (V)	J_{sc} (mA cm^{-2})	FF	PCE (%)[f]
DRCN5T[a]	0.92 ± 0.01	15.66 ± 0.22	0.68 ± 0.01	9.80 ± 0.28 (10.08)
DRCN6T[b]	0.92 ± 0.01	11.45 ± 0.25	0.58 ± 0.01	6.11 ± 0.22 (6.33)
DRCN7T[c]	0.90 ± 0.01	14.77 ± 0.10	0.68 ± 0.01	9.05 ± 0.25 (9.30)
DRCN8T[d]	0.86 ± 0.01	10.80 ± 0.18	0.68 ± 0.01	6.37 ± 0.13 (6.50)
DRCN9T[e]	0.81 ± 0.01	13.77 ± 0.14	0.68 ± 0.01	7.62 ± 0.24 (7.86)

[a]With thermal annealing at 120 °C for 10 min and solvent vapor annealing for 60 s. [b]With thermal annealing at 140 °C for 10 min. [c]With thermal annealing at 90 °C for 10 min; the data were obtained from ref 38. [d]With thermal annealing at 90 °C for 10 min. [e]With thermal annealing at 110 °C for 10 min. [f]The best PCEs are provided in parentheses.

The potentials were internally calibrated using the ferrocene/ferrocenium (Fc/Fc^+) redox couple (4.8 eV below the vacuum level). The energy levels of the highest occupied molecular orbitals (HOMOs) and lowest unoccupied molecular orbitals (LUMOs) calculated from the onset oxidation and reduction potentials are depicted in Figure 2c. The HOMO levels increase from −5.34 to −4.97 eV with increasing conjugation length, which is consistent with our DFT calculations (Table S3 in the SI). Their LUMO levels are similar, since the LUMO energies are largely dominated by the electron-deficient end groups.

Photovoltaic Properties. Solution-processed BHJ devices were fabricated using DRCN4T−DRCN9T as the electron donor with a conventional device structure of ITO/PEDOT:PSS/DRCN*n*T:$PC_{71}BM$/PFN/Al (where PFN is poly[(9,9-bis(3′-(*N*,*N*-dimethylamino)propyl)-2,7-fluorene)-*alt*-2,7-(9,9-dioctylfluorene)][48]). DRCN4T exhibited poor film quality and extremely low device performance of 0.24% (Table S4 in the SI), and thus, no further investigation was carried out for DRCN4T-based devices. The photovoltaic performances based on DRCN5T, DRCN6T, DRCN8T, and DRCN9T were systematically evaluated, and their optimal photovoltaic parameters together with those of DRCN7T for comparison are listed in Table 2.[38] The characteristic current density−voltage (*J*−*V*) curves for the optimized devices are shown in Figure 3a. The optimal devices based on DRCN5T gave an outstanding PCE of 10.08% (certified at 10.10%, with an average PCE of 9.80%) with an open-circuit voltage (V_{oc}) of 0.92 V, a fill factor (FF) of 0.69, and a high J_{sc} of 15.88 mA cm^{-2}; this PCE is the highest reported to date for single-junction SM-OPVs. The devices based on DRCN6T and DRCN8T exhibited moderate PCEs of 6.33% and 6.50%, respectively. As reported before, DRCN7T gave a PCE of 9.30%.[38] DRCN9T showed a relatively low V_{oc} of 0.82 V, due to its higher HOMO level, but a high FF of 0.69 and J_{sc} of 13.91 mA cm^{-2}. It is obvious that with the increase in the conjugation length, the V_{oc} decreased from ∼0.90 to ∼0.80 V, which is consistent with the trend of their HOMO levels. All of the optimal devices showed high FF values except that based on DRCN6T, and this reflects the fact that among all of the molecular structures only DRCN6T has a nonplanar structure (Figure S1 in the SI). Also, DRCN6T tends to have more edge-on packing in the active layer (see the GIXD study below). It is interesting to note that the devices based on DRCN5T, DRCN7T, and DRCN9T with axisymmetric chemical structures all exhibited much higher J_{sc} values (14−16 mA cm^{-2}) and thus higher PCEs than those based on DRCN6T and DRCN8T with centrosymmetric chemical structures ($J_{sc} \approx$ 11 mA cm^{-2}), which is also closely related to their different morphologies as discussed below. It has been reported that a large dipole moment change ($\Delta\mu_{ge}$) in going from the ground state (μ_g) to the excited state (μ_e) can lower the Coulombic binding energy of the exciton. This is expected to facilitate intramolecular charge dissociation and contribute to the high J_{sc}.[11,49] Time-dependent density functional theory (TD-DFT)-calculated values of $\Delta\mu_{ge}$ are listed in Table S1 in the SI. It can be seen that DRCN5T, DRCN7T, and DRCN9T with axisymmetric structures have larger $\Delta\mu_{ge}$ than DRCN6T and DRCN8T with centrosymmetric structures, This corresponds to the observation that solar cell devices based on DRCN5T, DRCN7T, and DRCN9T exhibit higher J_{sc} values than those based on DRCN6T and DRCN8T (Figure 3c).

The external quantum efficiency (EQE) curves of the optimal devices based on DRCN5T−DRCN9T are shown in Figure 3b. As shown by the EQE curves, broad spectral response across the wavelength range of 300−800 nm was observed for all of the devices. The EQE values for the DRCN5T-, DRCN7T-, and DRCN9T-based devices are clearly much higher than those of the DRCN6T- and DRCN8T-based devices. Especially, the EQE curve for the device based on DRCN5T exhibits a broader response and a clear peak at about 700 nm, consistent with its UV−vis absorption spectrum. The calculated J_{sc} values integrated from the EQE curves show a 3−5% mismatch compared with the J_{sc} values obtained from the devices' *J*−*V* curves.

Morphology Characterization. The morphologies of the optimal active layers were investigated by atomic force microscopy (AFM) and transmission electron microscopy (TEM). The AFM measurements (Figure S4 in the SI) showed that the films of DRCN5T−DRCN9T blended with $PC_{71}BM$

DOI: 10.1021/jacs.5b00305
J. Am. Chem. Soc. 2015, 137, 3886−3893

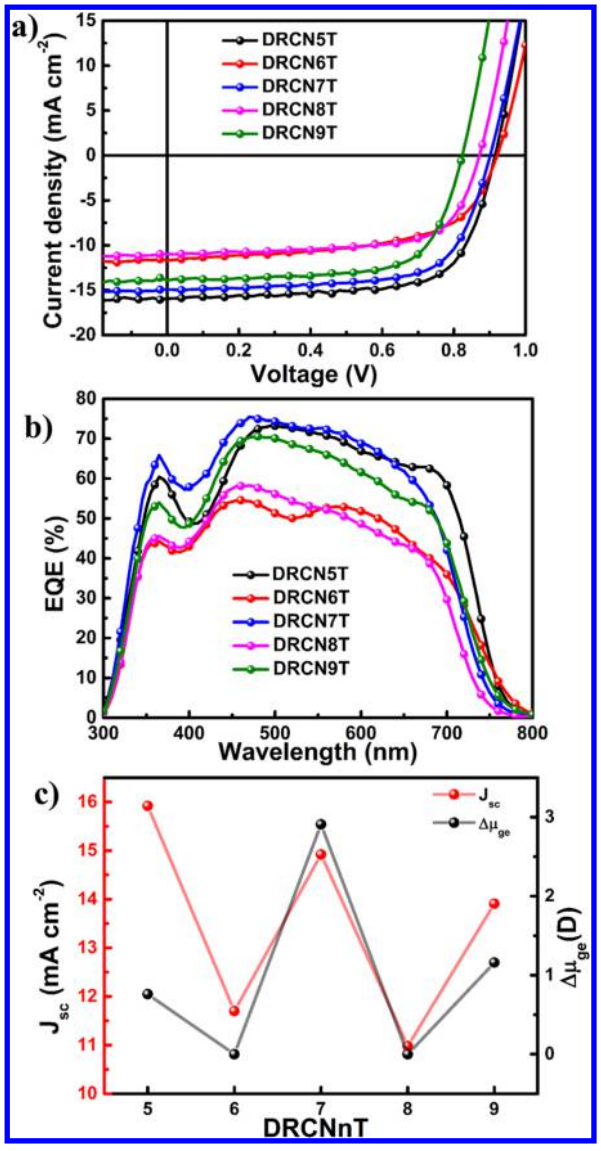

Figure 3. (a) Characteristic current density vs voltage (J–V) curves for the optimized devices under simulated AM 1.5 G irradiation (100 mW cm^{-2}). (b) External quantum efficiency (EQE) curves for the optimized devices. (c) Correlation between J_{sc} and dipole moment change ($\Delta\mu_{ge}$).

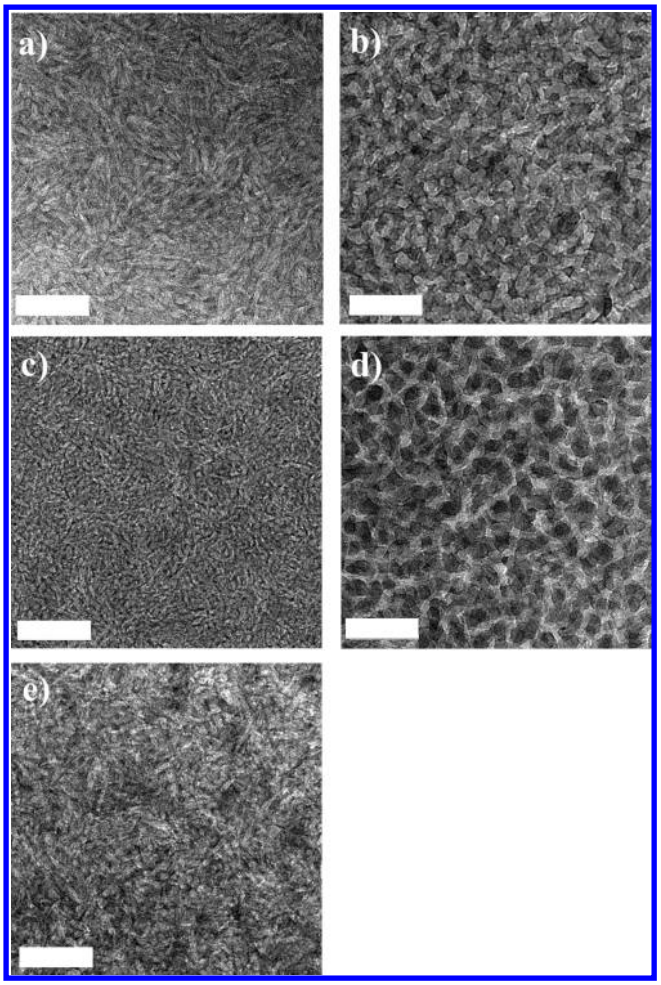

Figure 4. TEM images of optimal active layers based on (a) DRCN5T:$PC_{71}BM$, (b) DRCN6T:$PC_{71}BM$, (c) DRCN7T:$PC_{71}BM$, (d) DRCN8T:$PC_{71}BM$, and (e) DRCN9T:$PC_{71}BM$. Scale bars are 200 nm.

were smooth and uniform with similar and small root-mean-square (RMS) surface roughnesses of 0.80, 0.70, 0.39, 0.81, and 0.57 nm, respectively. The TEM images (Figure 4) show that DRCN5T/DRCN7/DRCN9T:PC71BM blend films gave bicontinuous interpenetrating networks with well-developed fibrillar structure,[50] and the widths of the fibrils were less than 20 nm. This is beneficial for exciton diffusion/dissociation and charge transport, which leads to a high J_{sc} and FF.[51,52] However, the blend films of DRCN6T and DRCN8T were characterized by much larger domains (~40 nm), which is unfavorable for exciton diffusion/dissociation and thus leads to lower J_{sc}.

The microstructures of the optimized pure and blend films, such as local molecular ordering/orientation and the intermolecular distances, were further characterized by two-dimensional (2D) GIXD (Figure 5 and Table 3). Out-of-plane line cuts are shown along with the 2D scattering profiles. Multiple higher-order (h00) reflections along the q_z direction were observed in all cases, indicative of long-range order and crystallinity in the pure and blend films.[53] For the pure films, DRCN5T and DRCN6T show a (010) reflection, characteristic of π–π stacking, along q_{xy} (i.e., in the plane of the film), indicating that DRCN5T and DRCN6T have a preferred edge-on orientation relative to the substrate. DRCN8T shows an azimuthally independent (010) peak, while the (010) reflection of DRCN9T is oriented along q_z, which is characteristic of a face-on orientation. The (100) peaks along the q_z direction for DRCN5T–DRCN9T are observed at 0.33, 0.34, 0.31, 0.33, and 0.32 Å^{-1}, respectively, corresponding to interchain distances of 19.0, 18.5, 20.3, 19.0, and 19.6 Å, respectively. For the blend films, the GIXD patterns with obvious (h00) reflections are similar to those observed in the pure films. DRCN5T, DRCN7T, DRCN8T, and DRCN9T show a more prominent face-on orientation, which favors charge transport and thus high FFs. However, for the DRCN6T blend film, a preferred edge-on orientation, in combination with its larger π–π stacking distance of 3.74 Å, is observed, which is unfavorable for charge transport, thus leading to a lower FF.[54] The hole mobilities of DRCN5T, DRCN7T, DRCN8T, and DRCN9T measured by the space-charge-limited current (SCLC) method (Figure S7 in the SI) are 6.54×10^{-4}, 5.91×10^{-4}, 5.77×10^{-4}, and 5.11×10^{-4} cm^2 V^{-1} s^{-1}, respectively, which are clearly higher than for

DOI: 10.1021/jacs.5b00305
J. Am. Chem. Soc. 2015, 137, 3886–3893

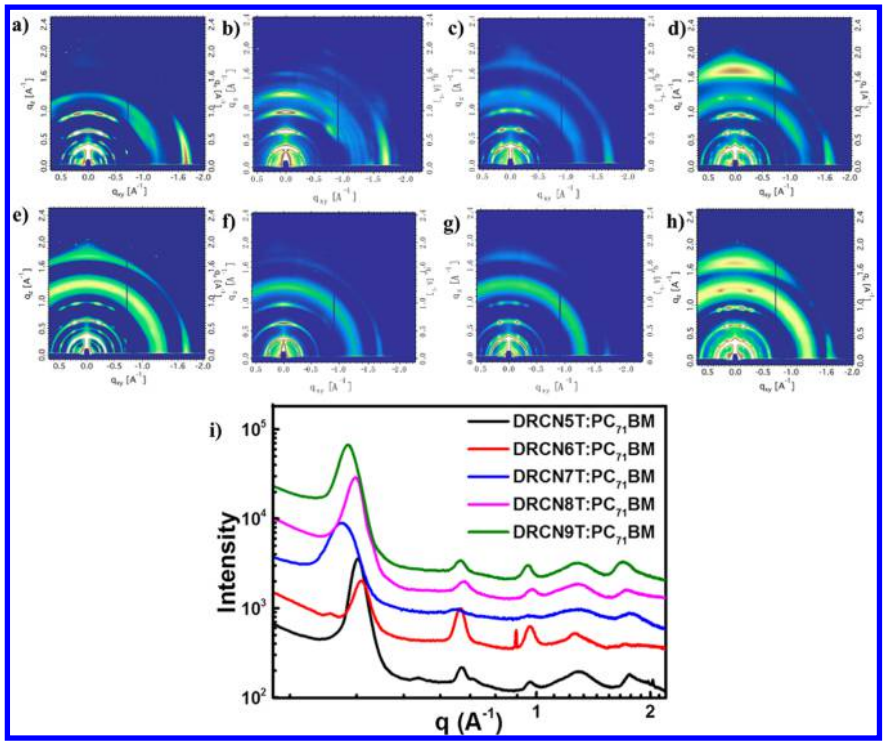

Figure 5. GIXD patterns for pure films of (a) DRCN5T, (b) DRCN6T, (c) DRCN8T, and (d) DRCN9T and blend films of (e) DRCN5T:$PC_{71}BM$, (f) DRCN6T:$PC_{71}BM$, (g) DRCN8T:$PC_{71}BM$, and (h) DRCN9T:$PC_{71}BM$. (i) Out-of-plane line cuts of the GIXD patterns for the blend films.

Table 3. Morphology Data from Out-of-Plane GIXD

	(100)		(010)		
active layer	q (Å^{-1})	d (Å)	q (Å^{-1})	d (Å)	face-on/ edge-on ratio
DRCN5T:$PC_{71}BM$	0.33	19.0	1.73	3.62	1.5
DRCN6T:$PC_{71}BM$	0.34	18.5	1.68	3.74	0.6
DRCN7T:$PC_{71}BM$	0.31	20.3	1.76	3.56	1.7
DRCN8T:$PC_{71}BM$	0.33	19.0	1.70	3.70	2.8
DRCN9T:$PC_{71}BM$	0.32	19.6	1.69	3.72	3.0

the DRCN6T (2.61×10^{-4} cm^2 V^{-1} s^{-1}) and are consistent with the GIXD results.

To probe the charge recombination in the optimal devices, the light intensity dependence of the J–V characteristics was measured. Figure 6 shows a linear dependence of the photocurrent density ($J_{ph} = J_L - J_D$, where J_L and J_D are the current densities under illumination and in the dark, respectively) on the light intensity (P) on a double logarithmic scale at both low and high effective voltages for all of the devices based on these molecules. The relationship between J_{ph} and P can be represented by the power-law equation $J_{ph} \propto P^{\alpha}$, where α is the recombination parameter, with $\alpha = 1$ corresponding to the absence of photocurrent loss due to bimolecular recombination.[55] It was shown that there was little charge recombination for the optimal devices based on DRCN7T.[38] Similar results were obtained for the optimal devices based on DRCN5T, DRCN8T, and DRCN9T, indicating little bimolecular recombination in these optimal devices, resulting in high FFs. For the optimal device based on DRCN6T, a lower α value of 0.89 was obtained, indicating pronounced bimolecular recombination and thus lower FF.[56−58]

CONCLUSION

We have designed and synthesized a series of simple oligomer-like small-molecule donor materials DRCN4T−DRCN9T with four to nine thiophene units in the backbones. The conjugation length and spatial symmetry have a significant impact on their optical and electrochemical properties and thus on the device performance. An odd−even effect in J_{sc} and PCE was observed. Higher values for DRCN5T, DRCN7T, and DRCN9T with an odd number of thiophene units were observed, which may be attributed to their large $\Delta\mu_{ge}$ and well-developed fibrillar network morphology due, more than likely, to their axisymmetric structures. Among them, DRCN5T exhibited an outstanding PCE of >10% (with a certified value of 10.10%), which is the highest PCE reported for single-junction SM-OPVs to date. Along with its very simple chemical structure and the easy synthesis procedure, which is certainly important for the possible future commercialization of OPVs, DRCN5T possesses a large potential for high-throughput applications. Because of the versatility and easy tuning of the structures, there are numerous opportunities to improve the design of the small molecules with higher performance.

EXPERIMENTAL SECTION

Materials Preparation. All reactions and manipulations were carried out under an argon atmosphere using standard Schlenk techniques. $PC_{71}BM$ was purchased from American Dye Source, Inc. PFN was obtained from SCUT. All of the materials were used as received unless otherwise specified. Synthesis details and characterization data for DRCN4T, DRCN5T, DRCN6T, DRCN8T, and DRCN9T, including NMR, CV, and other additional data, can be found in the SI.

Solar Cell Fabrication and Testing. The devices were fabricated with a structure of glass/ITO/PEDOT:PSS/donor:acceptor/PFN/Al. The indium tin oxide (ITO)-coated glass substrates were cleaned by

DOI: 10.1021/jacs.5b00305
J. Am. Chem. Soc. 2015, 137, 3886−3893

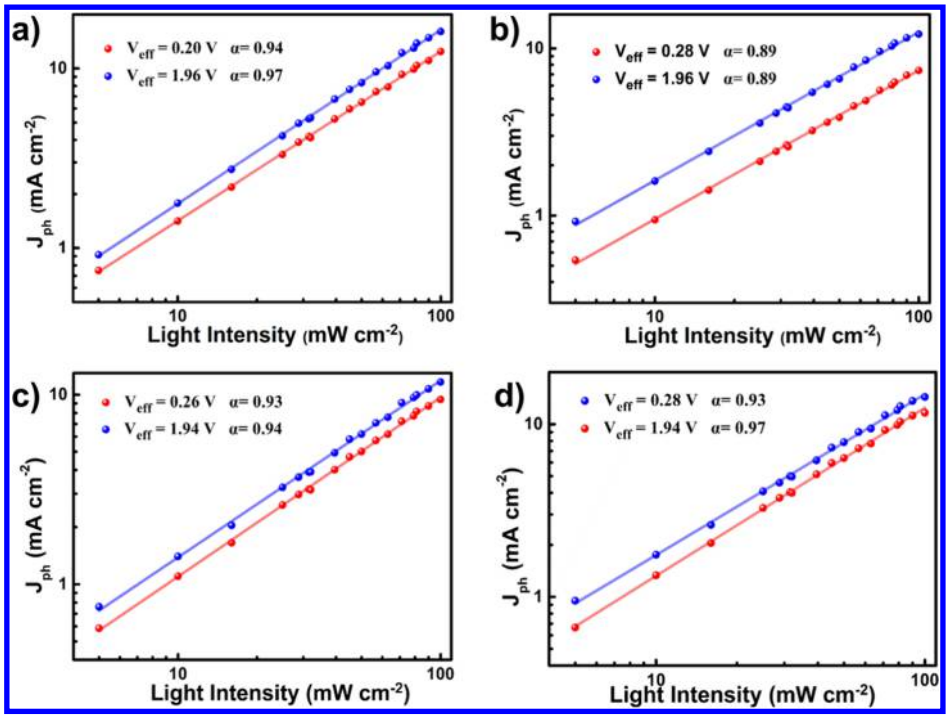

Figure 6. Double logarithmic plots of photocurrent density as a function of incident light intensity for devices based on (a) DRCN5T, (b) DRCN6T, (c) DRCN8T, and (d) DRCN9T. Lines represent the best power-law fits.

ultrasonic treatment in detergent, deionized water, acetone, and isopropyl alcohol under ultrasonication for 15 min each and subsequently dried by a nitrogen blow. A thin layer of PEDOT:PSS (Clevios P VP AI 4083, filtered at 0.45 μm) was spin-coated at 3000 rpm onto the ITO surface. After being baked at 150 °C for 20 min, the substrates were transferred into an argon-filled glovebox. Subsequently, the active layer was spin-coated from blend chloroform solutions with different ratios (weight-to-weight) of donor and $PC_{71}BM$ and then annealed at different temperatures for 10 min. For the devices based on DRCN4T, DRCN6T, DRCN8T, and DRCN9T, a thin layer of PFN and an 80 nm Al layer were deposited on the DRCN*n*T:$PC_{71}BM$ active layer under high vacuum (<2×10^{-4} Pa). For the devices based on DRCN5T, after thermal annealing the substrates were cooled to room temperature and then placed in a glass Petri dish containing 150 μL of chloroform for 60 s for solvent vapor annealing. The substrates were then removed, and a thin layer of PFN and an 80 nm Al layer were deposited under high vacuum (<2×10^{-4} Pa). The effective areas of the cells were 4 mm^2 as defined by shadow masks.

The $J-V$ curves for the photovoltaic devices were obtained using a Keithley 2400 source-measure unit. All of the masked and unmasked tests gave consistent results with relative errors within 5%. The photocurrent was measured under simulated 100 mW cm^{-2} AM 1.5G irradiation using an Oriel 96000 solar simulator calibrated with a standard Si solar cell. The average PCE was obtained using 50 devices under the same conditions.

The EQE values of the encapsulated devices were measured using a lock-in amplifier (SR810, Stanford Research Systems). The devices were illuminated by monochromatic light from a 150 W xenon lamp passing through an optical chopper and a monochromator. The photon flux was determined by a calibrated standard silicon photodiode.

Mobility measurements on the optimal blend films were carried out with the following diode structures: ITO/PEDOT:PSS/active layer/ETL/Au for holes by recording $J-V$ curves over the voltage range of 0−7 V. The charge carrier mobilities were calculated using the SCLC model:

$$J = \frac{9\varepsilon_0\varepsilon_r\mu_h V^2}{8L^3}\exp\left(0.89\beta\sqrt{\frac{V}{L}}\right)$$

in which J is the current density, L is the film thickness of the active layer, μ_h is the hole mobility, ε_r is the relative dielectric constant of the transport medium, ε_0 is the permittivity of free space (8.85×10^{-12} F m^{-1}), and $V = V_{appl} - V_{bi}$ is the internal voltage in the device, where V_{appl} is the voltage applied to the device and V_{bi} is the built-in voltage due to the relative work function difference of the two electrodes.

■ ASSOCIATED CONTENT

Supporting Information

Detailed synthetic procedures and characterization data for the new compounds and additional experimental results. This material is available free of charge via the Internet at http://pubs.acs.org.

■ AUTHOR INFORMATION

Corresponding Author

*yschen99@nankai.edu.cn

Author Contributions

⊥B.K., M.L., and Q.Z. contributed equally.

Notes

A patent (application no. CN2014100099426) has been filed for the materials.

The authors declare no competing financial interest.

■ ACKNOWLEDGMENTS

The authors gratefully acknowledge financial support from the MOST (Grants 2014CB643502 and 2012CB933401), NSFC (Grants 91433101, 51422304, and 51373078), NSF of Tianjin City (Grant 13RCGFGX01121), and PCSIRT (IRT1257). The morphological characterization of the active layers was supported by the DOE-funded Energy Frontier Research Center on Polymer-Based Materials for Harvesting Solar

DOI: 10.1021/jacs.5b00305
J. Am. Chem. Soc. 2015, 137, 3886−3893

Energy (DE-SC0001087). Portions of this research were carried out at the Advanced Light Source, Lawrence Berkeley National Laboratory, which is supported by the DOE, Office of Science, Office of Basic Energy Sciences. The authors also thank beamline BL14B1 (Shanghai Synchrotron Radiation Facility) for providing the beam time.

REFERENCES

(1) Service, R. F. *Science* **2011**, *332*, 293.
(2) You, J.; Dou, L.; Yoshimura, K.; Kato, T.; Ohya, K.; Moriarty, T.; Emery, K.; Chen, C.-C.; Gao, J.; Li, G.; Yang, Y. *Nat. Commun.* **2013**, *4*, No. 1446.
(3) Chen, J. D.; Cui, C.; Li, Y. Q.; Zhou, L.; Ou, Q. D.; Li, C.; Li, Y.; Tang, J. X. *Adv. Mater.* **2015**, *27*, 1035.
(4) Chen, C. C.; Chang, W. H.; Yoshimura, K.; Ohya, K.; You, J.; Gao, J.; Hong, Z.; Yang, Y. *Adv. Mater.* **2014**, *26*, 5670.
(5) Liu, Y.; Zhao, J.; Li, Z.; Mu, C.; Ma, W.; Hu, H.; Jiang, K.; Lin, H.; Ade, H.; Yan, H. *Nat. Commun.* **2014**, *5*, No. 5293.
(6) Kang, H.; Kee, S.; Yu, K.; Lee, J.; Kim, G.; Kim, J.; Kim, J. R.; Kong, J.; Lee, K. *Adv. Mater.* **2015**, *27*, 1408.
(7) Beaujuge, P. M.; Fréchet, J. M. J. *J. Am. Chem. Soc.* **2011**, *133*, 20009.
(8) Li, Y. *Acc. Chem. Res.* **2012**, *45*, 723.
(9) Zhou, H.; Yang, L.; You, W. *Macromolecules* **2012**, *45*, 607.
(10) Li, C. Z.; Chang, C. Y.; Zang, Y.; Ju, H. X.; Chueh, C. C.; Liang, P. W.; Cho, N.; Ginger, D. S.; Jen, A. K. *Adv. Mater.* **2014**, *26*, 6262.
(11) Lu, L.; Yu, L. *Adv. Mater.* **2014**, *26*, 4413.
(12) He, Y. J.; Chen, H. Y.; Hou, J. H.; Li, Y. F. *J. Am. Chem. Soc.* **2010**, *132*, 1377.
(13) Eftaiha, A.; Sun, J.; Hill, I.; Welch, G. *J. Mater. Chem. A* **2014**, *2*, 1201.
(14) He, C.; Su, S.; Xu, M.; Wu, H.; Cao, Y. *Nat. Photonics* **2012**, *6*, 591.
(15) Dou, L.; You, J.; Hong, Z.; Xu, Z.; Li, G.; Street, R. A.; Yang, Y. *Adv. Mater.* **2013**, *25*, 6642.
(16) Duan, C.; Zhang, K.; Zhong, C.; Huang, F.; Cao, Y. *Chem. Soc. Rev.* **2013**, *42*, 9071.
(17) Kong, J.; Hwang, I. W.; Lee, K. *Adv. Mater.* **2014**, *26*, 6275.
(18) Dang, M. T.; Wuest, J. D. *Chem. Soc. Rev.* **2013**, *42*, 9105.
(19) Ameri, T.; Li, N.; Brabec, C. J. *Energy Environ. Sci.* **2013**, *6*, 2390.
(20) Mei, J.; Bao, Z. *Chem. Mater.* **2014**, *26*, 604.
(21) Ye, L.; Zhang, S.; Huo, L.; Zhang, M.; Hou, J. *Acc. Chem. Res.* **2014**, *47*, 1595.
(22) Chochos, C. L.; Choulis, S. A. *Prog. Polym. Sci.* **2011**, *36*, 1326.
(23) Guo, X.; Baumgarten, M.; Müllen, K. *Prog. Polym. Sci.* **2013**, *38*, 1832.
(24) Mishra, A.; Bäuerle, P. *Angew. Chem., Int. Ed.* **2012**, *51*, 2020.
(25) Kyaw, A. K.; Wang, D. H.; Wynands, D.; Zhang, J.; Nguyen, T. Q.; Bazan, G. C.; Heeger, A. J. *Nano Lett.* **2013**, *13*, 3796.
(26) Kan, B.; Zhang, Q.; Li, M.; Wan, X.; Ni, W.; Long, G.; Wang, Y.; Yang, X.; Feng, H.; Chen, Y. *J. Am. Chem. Soc.* **2014**, *136*, 15529.
(27) Liu, Y.; Chen, C. C.; Hong, Z.; Gao, J.; Yang, Y. M.; Zhou, H.; Dou, L.; Li, G.; Yang, Y. *Sci. Rep.* **2013**, *3*, 3356.
(28) Roncali, J.; Leriche, P.; Blanchard, P. *Adv. Mater.* **2014**, *26*, 3821.
(29) Walker, B.; Kim, C.; Nguyen, T.-Q. *Chem. Mater.* **2011**, *23*, 470.
(30) Coughlin, J. E.; Henson, Z. B.; Welch, G. C.; Bazan, G. C. *Acc. Chem. Res.* **2014**, *47*, 257.
(31) Chen, Y.; Wan, X.; Long, G. *Acc. Chem. Res.* **2013**, *46*, 2645.
(32) Wessendorf, C. D.; Schulz, G. L.; Mishra, A.; Kar, P.; Ata, I.; Weidelener, M.; Urdanpilleta, M.; Hanisch, J.; Mena-Osteritz, E.; Lindén, M.; Ahlswede, E.; Bäuerle, P. *Adv. Energy Mater.* **2014**, *4*, No. 1400266.
(33) Liu, Y.; Zhou, J.; Wan, X.; Chen, Y. *Tetrahedron* **2009**, *65*, 5209.
(34) Liu, Y.; Wan, X.; Wang, F.; Zhou, J.; Long, G.; Tian, J.; Chen, Y. *Adv. Mater.* **2011**, *23*, 5387.
(35) Lin, Y.; Li, Y.; Zhan, X. *Chem. Soc. Rev.* **2012**, *41*, 4245.
(36) Fitzner, R.; Mena-Osteritz, E.; Mishra, A.; Schulz, G.; Reinold, E.; Weil, M.; Körner, C.; Ziehlke, H.; Elschner, C.; Leo, K.; Riede, M.; Pfeiffer, M.; Uhrich, C.; Bäuerle, P. *J. Am. Chem. Soc.* **2012**, *134*, 11064.
(37) Zhang, L.; Colella, N. S.; Cherniawski, B. P.; Mannsfeld, S. C.; Briseno, A. L. *ACS Appl. Mater. Interfaces* **2014**, *6*, 5327.
(38) Zhang, Q.; Kan, B.; Liu, F.; Long, G.; Wan, X.; Chen, X.; Zuo, Y.; Ni, W.; Zhang, H.; Li, M.; Hu, Z.; Huang, F.; Cao, Y.; Liang, Z.; Zhang, M.; Russell, T. P.; Chen, Y. *Nat. Photonics* **2015**, *9*, 35.
(39) Liu, X.; Sun, Y.; Perez, L. A.; Wen, W.; Toney, M. F.; Heeger, A. J.; Bazan, G. C. *J. Am. Chem. Soc.* **2012**, *134*, 20609.
(40) Li, W.; Yang, L.; Tumbleston, J. R.; Yan, L.; Ade, H.; You, W. *Adv. Mater.* **2014**, *26*, 4456.
(41) Liu, X.; Sun, Y.; Hsu, B. B.; Lorbach, A.; Qi, L.; Heeger, A. J.; Bazan, G. C. *J. Am. Chem. Soc.* **2014**, *136*, 5697.
(42) Dang, M. T.; Hirsch, L.; Wantz, G.; Wuest, J. D. *Chem. Rev.* **2013**, *113*, 3734.
(43) Liu, F.; Chen, D.; Wang, C.; Luo, K.; Gu, W.; Briseno, A. L.; Hsu, J. W.; Russell, T. P. *ACS Appl. Mater. Interfaces* **2014**, *6*, 19876.
(44) He, G.; Li, Z.; Wan, X.; Zhou, J.; Long, G.; Zhang, S.; Zhang, M.; Chen, Y. *J. Mater. Chem. A* **2013**, *1*, 1801.
(45) Fitzner, R.; Elschner, C.; Weil, M.; Uhrich, C.; Körner, C.; Riede, M.; Leo, K.; Pfeiffer, M.; Reinold, E.; Mena-Osteritz, E.; Bäuerle, P. *Adv. Mater.* **2012**, *24*, 675.
(46) Schrader, M.; Fitzner, R.; Hein, M.; Elschner, C.; Baumeier, B.; Leo, K.; Riede, M.; Bäuerle, P.; Andrienko, D. *J. Am. Chem. Soc.* **2012**, *134*, 6052.
(47) Koch, F. P.; Smith, P.; Heeney, M. *J. Am. Chem. Soc.* **2013**, *135*, 13695.
(48) He, Z.; Zhong, C.; Huang, X.; Wong, W.-Y.; Wu, H.; Chen, L.; Su, S.; Cao, Y. *Adv. Mater.* **2011**, *23*, 4636.
(49) Carsten, B.; Szarko, J. M.; Lu, L.; Son, H. J.; He, F.; Botros, Y. Y.; Chen, L. X.; Yu, L. *Macromolecules* **2012**, *45*, 6390.
(50) Li, W.; Hendriks, K. H.; Furlan, A.; Roelofs, W. S.; Wienk, M. M.; Janssen, R. A. *J. Am. Chem. Soc.* **2013**, *135*, 18942.
(51) Brabec, C. J.; Heeney, M.; McCulloch, I.; Nelson, J. *Chem. Soc. Rev.* **2011**, *40*, 1185.
(52) Huang, Y.; Kramer, E. J.; Heeger, A. J.; Bazan, G. C. *Chem. Rev.* **2014**, *114*, 7006.
(53) Muller-Buschbaum, P. *Adv. Mater.* **2014**, *26*, 7692.
(54) Liu, F.; Gu, Y.; Shen, X.; Ferdous, S.; Wang, H.-W.; Russell, T. P. *Prog. Polym. Sci.* **2013**, *38*, 1990.
(55) Lenes, M.; Morana, M.; Brabec, C. J.; Blom, P. W. M. *Adv. Funct. Mater.* **2009**, *19*, 1106.
(56) Mandoc, M. M.; Veurman, W.; Koster, L. J. A.; de Boer, B.; Blom, P. W. M. *Adv. Funct. Mater.* **2007**, *17*, 2167.
(57) Guerrero, A.; Loser, S.; Garcia-Belmonte, G.; Bruns, C. J.; Smith, J.; Miyauchi, H.; Stupp, S. I.; Bisquert, J.; Marks, T. J. *Phys. Chem. Chem. Phys.* **2013**, *15*, 16456.
(58) Proctor, C. M.; Kim, C.; Neher, D.; Nguyen, T.-Q. *Adv. Funct. Mater.* **2013**, *23*, 3584.

DOI: 10.1021/jacs.5b00305
J. Am. Chem. Soc. 2015, 137, 3886−3893